Simulation of the GOx / GCH4 multi-element combustor and study of the turbulent diffusion coefficients influence

By E. Strokach, I. Borovik and O. Haidn †

Department of Rocket engines, Moscow Aviation Insitute, Volokolamskoe sh. 4, 125993, Moscow

Within the SFB-TRR 40 Summer Program 2019 framework the modeling of the processes in an experimental rocket combustor was made. The gaseous oxygen (GOX) and methane (GCH4) operating thruster geometry and the test data were taken from the previous experimental studies at the Chair of turbomachinery and Flight propulsion of the TUM. The 3D RANS approach using a 60° sector as a simulation domain was used for the studies. The primary goals of the research were to examine the effect of turbulent diffusion coefficients variation, such as turbulent Prandtl and Schmidt numbers, whereas two algebraic variable turbulent Prandtl approaches were implemented, and to study the influence of radiation heat transfer (RHF). Also, the dependence of the results on turbulence modeling was studied. Finally, an adiabatic Flamelet approach was compared to the enhanced one global reaction Eddy-dissipation approach. The normalized and absolute pressure, the integral and segment averaged heat flux were taken as experimental reference for the comparison with the numerical results. The behavior of the modeling approaches was discussed and best performing models were chosen. The obtained numerical results showed good agreement with the experimental data, having a small underestimation for pressures of around 2.9%, whereas for the wall heat flux a larger final error was achieved, which is addressed to the experimental setup, which had been reported by other researchers before. The plans for future research were also announced, especially concerning turbulence diffusion and radiation modeling.

1. Introduction

The design and optimization of rocket propulsion devices is a complex procedure which now contains the numerical simulation of flow and tough physical phenomena as a very important part of the process. This is mainly due to the significant reduction of the cost and time needed for overall testing, production and development cycle. The main criterions that show if the code can be applied for rocket thrusters are wall heat transfer, combustion efficiency, specific impulse and pressure representation. The tool should both accurately predict the parameter distribution inside the combustor and satisfy the engineering needs such as robustness and (as much as can) low computational requirements. Numerical codes, therefore, should be validated for the criterions in question and the most suitable models of physical phenomena should be chosen. For the recent years, at the Chair of Turbomachinery and Flight Propulsion (LTF) at the Techni-

† Technische Universität München, Boltzmannstr. 15, 85748 Garching b. München

cal University of Munich several rocket propulsion framework studies have been carried out.

Among these, a GCH4/GOx multi-element injector test case was chosen to validate the numerical setting during the SFB/TRR 40 Summer Program 2019. The reason to choose this experiment was not only the well-described and suitable for numerical verification setting, but also its spread among other research groups which helps to efficiently compare and choose the proper approaches. A paper by Silvestri et al. [1, 2] gives the detailed data concerning the test bench and experimental setting and a short description is given in Section 2.

In this paper the results of numerical studies of the group from Moscow aviation institute, Rocket propulsion department are presented. One of the main concepts of this research project was checking the applicability the relatively robust and effortless models for the studied physical processes, which could be then used in the routine engineering design optimization process. The studies were mainly aimed at the determination of the influence of turbulent diffusion coefficients, such as the turbulent Prandtl and turbulent Schmidt numbers. The effect of turbulence models is also studied. To observe the influence of radiative heat flux, the Gray and weighted sum of gray gases (WSGG) models were examined. The effect of combustion modeling approaches was also explored. Section 3 gives an overview of the models used and the computational setup. The results and discussion around them are presented in Section 4. Section 5 includes a conclusion and outcomes of the results and describes the future studies and perspective to improve the numerical setting.

2. The test case

The chosen test case was developed and operated as part of the Transregio SFB-TR 40 program. It includes seven coaxial gaseous methane and gaseous oxygen injectors which allows for the injector-injector and injector-wall interaction investigation that determines the overall combustion performance and wall heat transfer. The view of the studied combustion chamber is shown on Fig. 1. One of the features of the design is that it contains of four cylindrical water-cooled segments and one nozzle segment allowing to determine the wall heat flux. The total length of 381 mm makes it possible for the injected coaxially jets to mix and react. The 30 mm chamber diameter and the injector head configuration makes it at some sense similar to the GCH4/GOx 6-injector MAI test engine [3], which, however, has much smaller axial size and a little higher radial size.

For the present study an operating point according to the mixture ratio 2.65 and the mean pressure of 18.3 bar was chosen. The experimentally determined data includes heat flux for each segment, mean pressure, wall pressure distribution, wall temperatures and methane / oxygen flow rates. References [1, 4, 5] give full information of the experimental data available.

Generally, the test setup provides a large field to customize and amplify the numerical approaches used in terms of both pressure and heat flux. An interesting aspect here is that due to the ability to use different oxidizer to fuel ratios, various fuels and implementation of the wall film cooling it makes possible to overview the influence of the configurations and helps to make the numerical approaches more universal.

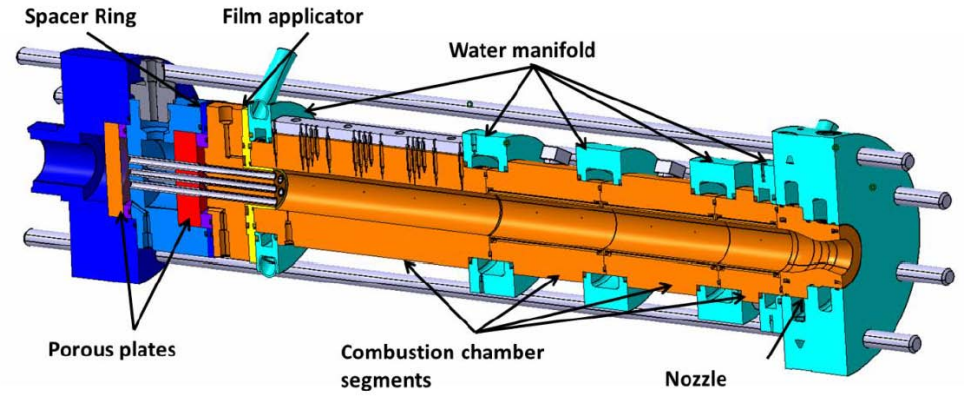

FIGURE 1. View of the studied thrust chamber [1, 2]

3. Numerical setup

The numerical simulations were carried out with use of the 3D Ansys CFX [4] coupled algebraic multigrid solver. The Favre-averaged equations were solved in a steady-state setting.

3.1. *Simulation domain*

The domain chosen for the computations resolved the 60° sector of the combustor, which included 1 peripheral injector and 1/6 of the central injector. To make use of the developed velocity profile at the injection point, the injector pipes were also included. As described on Fig. 2, the symmetry boundaries were applied to the planes corresponding to $\pm 30^\circ$ from the injectors radial position. This symmetrical approach has already been widely used in the rocket combustor studies, both the particular and the others [5–8]. The experimental mass flows and temperatures were defined for the fuel and oxidizer inlets and an "opening" type for the outlet boundary was set. At the thruster wall, the non-slip condition with the experimental temperature profile shown on Fig. 3 was reproduced. The other wall faces were modeled with a no-slip adiabatic approach. Due to the previously detected ambiguities in the nozzle heat flux estimations and need to account for the conjugate heat transfer [5, 7], no comparison between the experimental and CFD data was applied. The nozzle temperature was set equal to the last value of the temperature profile in the cylindrical part.

The approximate size of 3.4 M hexahedral cells was chosen for the numerical grid after a convergence study based on the average pressure and integral wall heat flux criterions. Most of the research on the present and other combustors had a resolving-to-the-wall grid to satisfy the $y^+ \approx 1$ condition [5–9]. Some groups focus on the development of special wall-functions, but it is mainly coupled with LES turbulence modeling [9–17]. In this study, one of the main issues was to check if the wall function approach can be applicable with RANS for the wall heat flux estimation which would make the optimization routine computations in industry more fast and easy. Thus, a $y^+ \approx 45 \ldots 240$ mesh was used. On the Fig. 4, a view on some of the mesh details is shown.

3.2. *Numerical models*

During the current research project different studies were proposed. To study the influence of the turbulent diffusion coefficients, the turbulent Prandtl and turbulent Schmidt

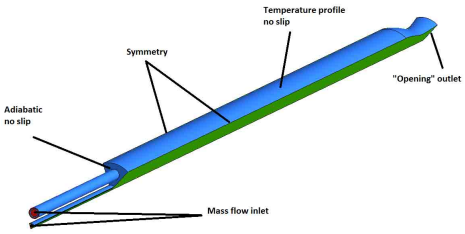

FIGURE 2. Domain and boundary conditions

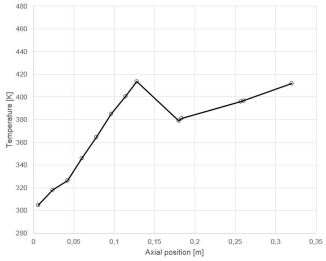

FIGURE 3. Axial wall temperature profile [1, 2]

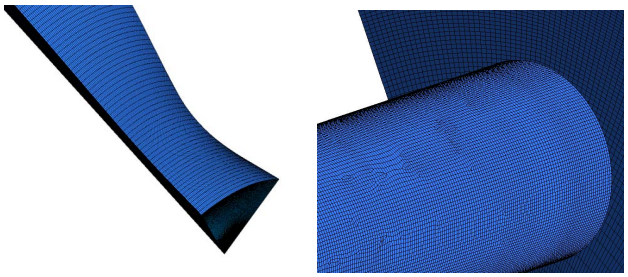

FIGURE 4. a, b View of the mesh details

variations were applied. Also two algebraic variable Prandtl models were utilized, which is observed in section 3.2.1. Two combustion models were studied – the adiabatic Flamelet and an enhanced Eddy-dissipation approach which is in details observed in section 3.2.2. The investigation of turbulence models influence included the SST, k-epsilon and BSL EARSM models which is in short presented in section 3.2.3 and is crucial for accurate estimation of the eddy viscosity [22–25]. What is more, three approaches for the radiative heat transport into the simulation, three approaches transfer were compared – the no radiation, the P1 model with the Gray gas approach and the Weighted sum of gray gases method. The WSGG model was previously implemented into CFX which is described in section 3.2.3.

3.2.1. *Turbulent Prandtl and turbulent Schmidt number studies*

There have been already some studies done making approximations of the turbulent Schmidt and Prandtl for the similar geometry and conditions [5–10]. However, all of them used the "resolved to the wall" approach with RANS, did not take radiation into account and did not use locally variable turbulent Prandtl approaches. To study such effects, three constant values – 0.3,0.6,0.9 and two algebraic models for the variable turbulent Prandtl number were chosen. These two models had been previously studied by D. Yoder [18] and showed relatively good performance (compared to the differential models studied) for the near-wall, jet and pipe flows. Here, one reason to use the algebraic approaches was their robustness and simplicity. The Kays and Crawford (3.2) and Wassel and Catton (3.1) models [19, 20] were implemented into CFX and studied.

$$Pr_t = \frac{C_3}{C_1 P_r}\left[1-\exp\left(\frac{-C_4}{\mu_t/\mu_l}\right)\right]\left[1-\exp\left(\frac{-C_2}{\left(\frac{\mu_t}{\mu_l}\right)P_r}\right)\right]^{-1} \tag{3.1}$$

$$Pr_t = \left\{ \frac{1}{2Pr_{T\infty}} + \frac{CPe_t}{\sqrt{Pr_{T\infty}}} - (CPe_t)^2 \left[1 - \exp\left(\frac{-1}{CPe_t \sqrt{Pr_{T\infty}}} \right) \right] \right\}^{-1} \tag{3.2}$$

Here, $C_1 = 0.21$, $C_2 = 5.25$, $C_3 = 0.2$, $C_4 = 5$, Pr is the molecular Prandtl number, μ – eddy viscosity, μ_l – dynamic viscosity, $C = 0.3$, $Pr_{T\infty} = 0.85$ and Pe_t and is the turbulent Peclet number.

To evaluate the effect of the turbulent Schmidt number, the values of 0.3, 0.6 and 0.9 were taken. A variable turbulent Schmidt model [21] depending on the local turbulent variables had been also implemented, but because of the lack of time the variable turbulent Schmidt modeling was not performed.

3.2.2. *Combustion models*

Two general approaches were used to model chemical reactions. One is the adiabatic Flamelet approach, which underlying theory is very well described in Ansys CFX Theory guide [4, 25, 26]. Its main advantage is high computational performance while still considering full kinetics due to only two scalars to transport - the mixture fraction and mixture fraction variance. The turbulence-chemistry interactions were accounted for by the scalar dissipation rate. The C1 CH4/O2 kinetics was used to create a flamelet database in CFX-RIF. In rocket thrusters, a high axial pressure change is present from the injector faceplate to the nozzle orifice, where pressure changes from the injection pressure to the ambient. Also, during a startup transient process, the pressure in the injector area changes rapidly from ambient to the steady-state values. To study the effect of the initial pressure, two flamelet libraries were used and compared, being addressed here as flamelet-1 and flamelet-2 for 1 atm and 20 atm correspondingly.

Another combustion model used here was an enhanced eddy-dissipation approach [4, 27]. The global reaction includes additional species – OH, CO, H, H_2, O. The procedure to derive the global reaction equation is as follows: a) a thermodynamic 1-D calculation is done in Rocket propulsion analysis software [27], b) the species with largest molar fraction are taken and molar fractions are used as the initial stoichiometric coefficients for the global reaction, c) the left-side (CH_4 and O_2) and the right-side coefficients (for H or others) are changed to satisfy the mass balance. Due to only one global reaction it remains fast and relatively robust while still accounting for high temperature dissociation and production of most participating species. The final global reaction is presented below (3.3).

$$\begin{gathered} 0.2789274[CH_4] + 0.5576753[O_2] = \\ = 0.147891[CO] + 0.131036[CO_2] + 0.028828[H] + 0.0597107[H_2] + \\ + 0.433845[H_20] + 0.0260146[O] + 0.072879[O_2] + 0.0997694[OH]. \end{gathered} \tag{3.3}$$

3.2.3. *Turbulence models*

The turbulence model effect was also studied. Previously, there had been some comparison of turbulence models provided [5, 10]. Sufficient influence of turbulence modeling on the mean pressure was noticed which was due to better or worse mixing efficiency. The present research, however, includes effects of turbulence anisotropy due to explicit algebraic approach. The turbulence models compared here BSL EARSM, k-omega SST and k-epsilon [4]. The BSL EARSM and k-omega SST use the automatic wall treatment technique which automatically switches from law-of-the-wall to low-Re simulation. In this study, as the mesh was unique for all models studied, the near wall modeling was based on the wall function approach.

3.2.4. *Radiation models*

The high and non-homogenous temperature values inside the rocket combustors compel researchers to account for radiative heat transfer. Here, to study its influence, several cases were numerically compared: the non-radiative and two radiative ones. The radiative simulations were done with the Gray spectral model and the WSGG method. The P1 differential model was used due to its applicability to wide range of optical thicknesses and its robust behavior during simulations. No scattering was considered in this study as no particles were introduced; the studies of radiation heat transfer without scattering had been done for gaseous fuels before, and gave decent results [28]. The default Gray spectral model was used, whereas the implemented WSGG references to the paper by Centeno et.al. [29]. In this paper, the authors introduced a four-gray-gases WSGG model with weighting factors for each gray gas derived as a polynomial function of temperature. The absorption coefficients depend upon the partial pressures of most radiating species, H_2O and CO_2.

4. Results and discussion

In this section the results of CFD simulations are given and compared to the measured data. The radiation approach, turbulence model and turbulent Prandtl/Schmidt effects are discussed. Also the TCC values influence is described and combustion models are compared. Despite a lot of numerical data was produced, the final outlook of the observations is expected to give specific outline and recommendations for use in future simulations and for enhanced studies.

4.1. *Turbulent Prandtl number effect*

Here, the computed average heat flux profile and pressure distribution for three constant turbulent Prandtl values and two locally derived algebraic approaches are compared to the measured ones. Fig. 5 and Fig. 6 show the axial absolute and normalized pressure values for a band of models. For this study the following fixed features were used: the flamelet 1 model, the SST turbulence model, P1 WSGG spectral radiation approach. It can be noticed that the turbulent Prandtl value mostly affects the normalized lines, and the lower Pr_t is, the more concave the profile looks along the thruster. The constant values about 0.9, however, give the same pressure values as variable turbulent Prandtl models. The segment average heat flux profile comparison (Fig. 7) also shows some interesting points. The heat flux increases with decreasing the turbulent Prandtl, and the results derived with the constant value of 0.9 are in the vicinity of the heat fluxes obtained with the algebraic variable models. Some additional studies showed that this effect keeps for cases without radiation modeling and for any turbulence models. The integral heat fluxes and radiative to total ratio outlined in Table 1 indicate this dependence; another interesting thing is that the radiative heat flux fraction increases with the increasing turbulent Prandtl and at the level of 0.9 it is the same as for the algebraic turbulent Prandtl models. The increasing tendency is easily explained by the change of the convective heat flux fraction due to Prandtl increase, whereas the similarity of the turbulent Prandtl value of 0.9 with the algebraic locally variable approaches shows that this value (and values in the vicinity) is dominant in the studied thruster. These approaches also give the best fit with the test measurements.

This is proved by turbulent Prandtl fields for the Kays and Crawford and Wassel and Catton formulations (Fig. 8 and 9). The KC model gives the turbulent Prandtl variation

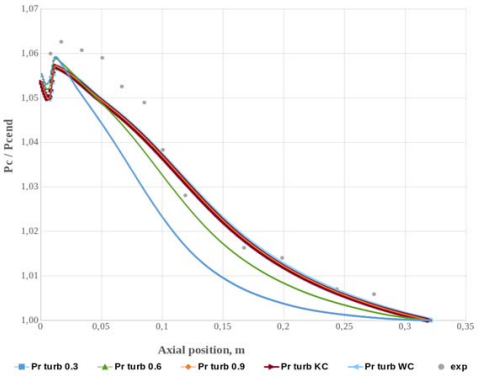

FIGURE 5. Axial normalized pressure.

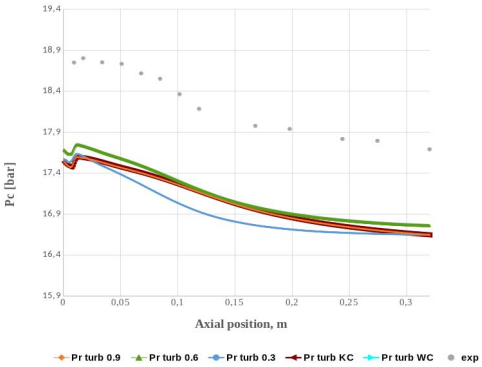

FIGURE 6. Absolute pressure axial distribution.

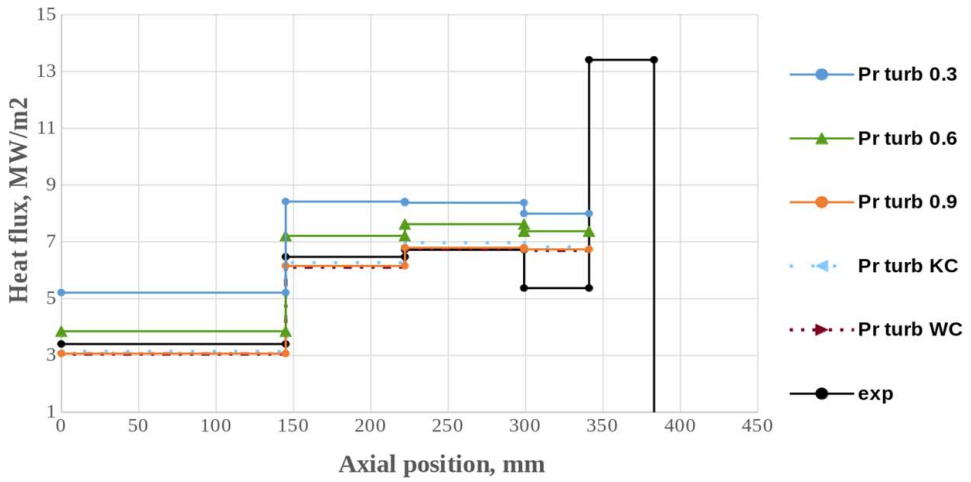

FIGURE 7. Heat flux segment average distribution

	Turbulent Prandtl number					
	0.3	0.6	0.9	KC	WC	exp
Integral, MW	0.2247	0.189	0.16248	0.16542	0.1614	0.16
Radiative/Total	0.1840	0.198	0.20800	0.20800	0.2090	—

TABLE 1. Turbulent Prandtl number

of 0.84 - 0.89 while the WC model's prandtl number varies from 0,87 to 0.94. In general, this results correlate with the approximations taken by other authors [5–8, 10] and make us more sure that the assumptions to take the values of 0.85-0.9 were valid. However, the variable models have large advantages over the constant values approaches - they are universal for a vast variety of injection schemes and are still robust – there had been no convergence difficulties or slowdown during simulations. Therefore, both KC and WC approaches should be recommended for engineering implementation and for future advanced research.

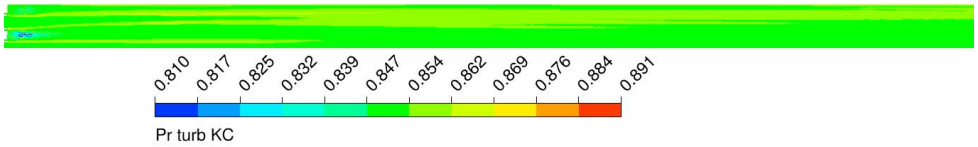

FIGURE 8. Turbulent Prandtl field given by the Kays and Crawford model

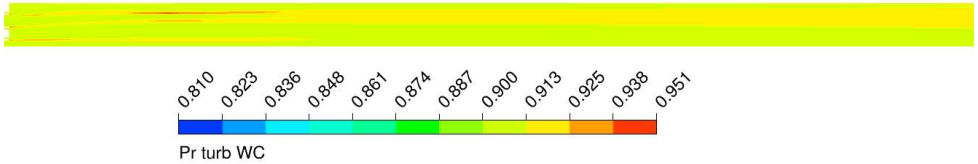

FIGURE 9. Turbulent Prandtl field given by the Wassel and Catton model

4.2. *Radiative heat transfer modeling*

As already mentioned, the Gray spectral model and the WSGG model were used to account for radiative heat flux (RHF). The Flamelet-1, default turbulent Prandtl number and the SST model were used for this study. The normalized pressure plot shows no effect of RHF, neither Gray or WSGG approach, on the axial distributions. Oppositely, the RHF changes the absolute pressure values by 0.25 bar and by 0.5 bar for WSGG and Gray spectral models respectively. This is due to the loss of heat from the flame-front and transport to the wall, which is shown on the heat flux plot (Fig. 10 - 12). A notable thing is that the Gray model gives an overestimated by 12.5 % integral heat flux, whereas a no-radiation case leads to underestimating it up to 15 %. Some kind of compromise is found by the WSGG approach, which gives very close to experimental values of the integral heat flux, though the profile has some discrepancies in the first and last segments (Table 2). The overestimation of the heat flux by the Gray approach is also seen from the radiative/total heat flux ratio. This value reaches 32 % for the Gray model, while only 20 % is given by the WSGG. Thellmann in his thesis [28] pointed out that the radiative amount of heat flux calculated with the WSGG models would be around 9-10 % when estimating it for the Space Shuttle main engine (SSME) nozzle. However, the average pressure reached 190-200 bar, whereas in this case we deal with much lower pressures, and the radiative fraction for these conditions might be much higher. Despite the fact that relative amount of RHF is still not undisputable, the WSGG model gives the best fit and should be used for further simulations.

The inclusion of the RHF decreases the flame temperature, not depending on the spectral model used, and does not affect the flame shape.

The WSGG model not only predicts much lower values, but also the most emitting area is sufficiently smaller. These effects derive from the CO_2 and H_2O mass fractions as the WSGG radiation intensity is dependent on these species' concentrations.

The same effects keep for the Enhanced EDM combustion model, different turbulent models and turbulent Prandtl numbers.

4.3. *Turbulence modeling study*

The study of turbulence model influence was done with the following modeling features same for all calculations: the flamelet-2 combustion model, the default turbulent Prandtl number (0.9) and to make the results cleaner, no radiation was considered for

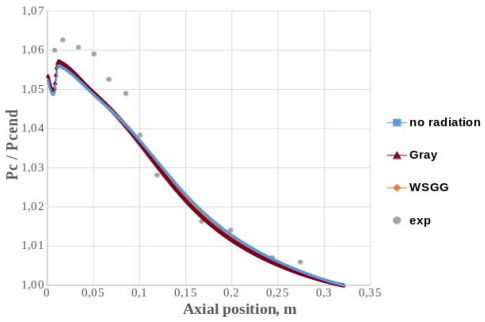

FIGURE 10. Normalized axial pressure distribution.

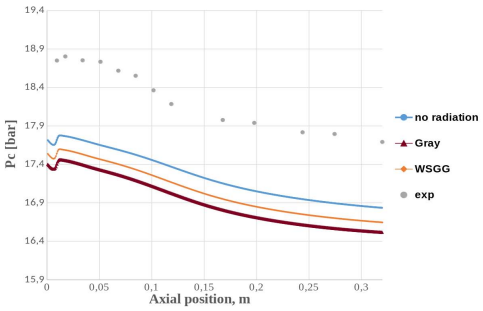

FIGURE 11. Absolute pressure axial distribution.

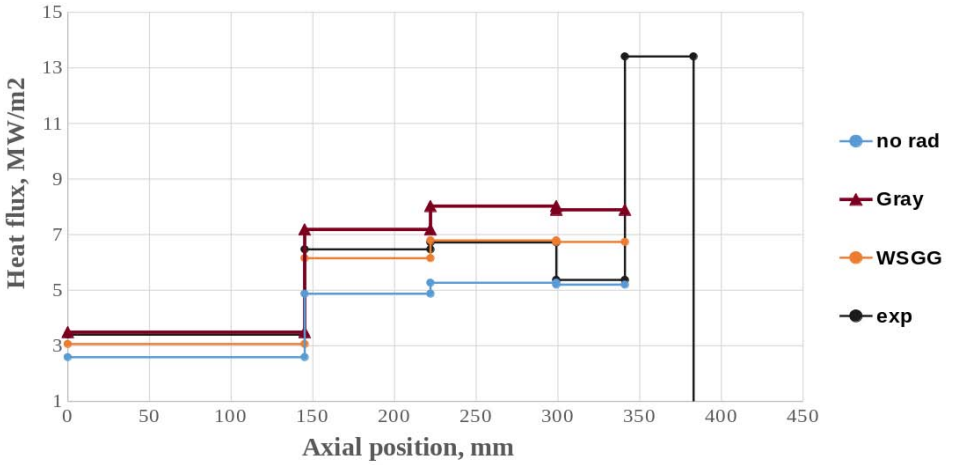

FIGURE 12. Segment average heat flux distribution.

	Radiation model			
	No rad	Gray	WSGG 4 gases	exp
Integral, MW	0.1293	0.193	0.16542	0.16
Radiative/Total	0	0.3221	0.208	—

TABLE 2. Radiation model

in these simulations. Generally, three models were studied – the k-omega SST, the k-epsilon model (applying a scalable wall function) and the BSL EARSM model to account for turbulence anisotropy. Initially, the k-omega based BSL RSM and k-epsilon based SSG Reynolds stress models were planned to be under study also, but the SSG model showed highly unstable convergence behavior and made it challenging to get the converged data until the end of the project. The BSL RSM simulations, on the opposite, converged smoothly, but resulted in one order unphysically higher eddy viscosity for the central injector, which had not been noticed for other turbulence models (even for partially converged SSG case). The cause of this is still under question, but the probable

reason is the symmetry boundary conditions for the 1/6 sector of the central injector or ambiguity in the turbulence boundary conditions. In future, periodic boundary conditions should be applied and a study of boundary conditions should be planned to explore the influence.

The normalized pressure profiles (Fig. 13) show better prediction of the pressure peak in the first 100 mm after the injector by the SST model. The K-epsilon and BSL EARSM models similarly calculate the absolute pressures, whereas the SST model gives 0.2 bar less pressure on average. This behavior is correlating with the results of other authors [5, 6, 10] as the k-epsilon model usually showed better mixing and higher pressures. Here, this effect is also addressed to the higher eddy viscosity given by the k-epsilon model and thus more intensive mixing. The BSL EARSM model shows even higher eddy viscosities in the near-injector region and in the back of the cylindrical part, which results in augmented pressure in these areas. The BSL EARSM gives higher heat fluxes in the first segment and slightly less values in the middle. The heat production by the SST model is the smallest among all described models (Fig. 14 and 15). Giving both more convenient results for the pressure and quite nice fit for the heat flux among other models, the BSL EARSM model is recommended for further use.

4.4. *Turbulent Schmidt number effect*

This section presents the study of different turbulent Schmidt numbers with the EDM global reaction mechanism (described in section 3.2.2), the SST model employed. No radiative heat transfer is included. Fig. 16 and 17 describe the axial pressure distribution, where some obvious effect is seen. The experimental normalized pressure is best fitted by the turbulent Schmidt of 0.6, as in the first 100 mm of the combustor it shows highest combustion performance, still underestimating it. For the rest of the combustor, this value of turbulent Schmidt also gives the best fit with the test. The absolute pressure values do not vary much for turbulent Schmidt numbers of 0.9 and 0.6, and the turbulent Schmidt 0.3 shows unrealistic behavior as well as for the normalized pressure. The heat flux plot (Fig. 18) indicated that the turbulent Schmidt of 0.6 shows more physical distribution comparing to Sc 0.3, and gives better fit compared to Sc 0.9. Overall, nevertheless Sc 0.3 gives best agreement with the test integral heat flux, and based on the comparison for pressure and segment average heat flux profiles, the turbulent Schmidt around 0.6 can be considered as suitable for the present operation conditions. The variable Schmidt number models are needed though to extend the results on other operation conditions.

4.5. *Combustion model effect*

An impact of three combustion models is presented in this section. The SST turbulence model, default turbulent Prandtl number (0.9) were used and no radiation was accounted for while the Flamelet-1, Flamelet-2 and EDM combustion approaches were studied. The variation of these approaches does not have influence on the normalized pressure distribution, while significantly effects the absolute values (Fig. 19, 20). The Flamelet-2 gives the highest absolute pressures, which are around 0.6 bar lower than the experimental ones and around 0.3 bar higher than Flamelet-1. This was expected as the Flamelet-2 model was created for fuel and oxidizer reacting at 20 bar, which is far closer to the experimental manifold pressures. The enhanced EDM approach gives 1.5 bar less than experimental pressures in average. Such low pressure cannot be addressed to wall heat loss – the EDM approach provides only slightly higher integral heat flux than both Flamelet models, and most of heat is transferred to the wall in the 4th segment, which experimental data is still ambiguous. The Flamelet 1 and 2 (Fig. 21) ap-

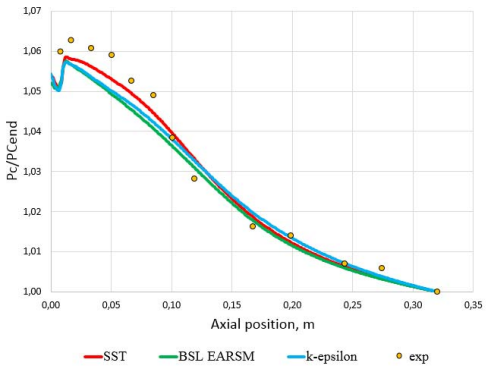

FIGURE 13. Normalized axial pressure distribution for various TCC.

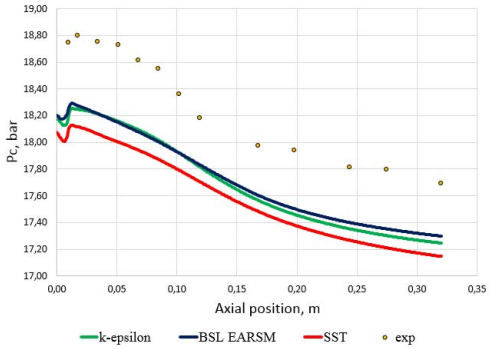

FIGURE 14. Absolute pressure axial distribution.

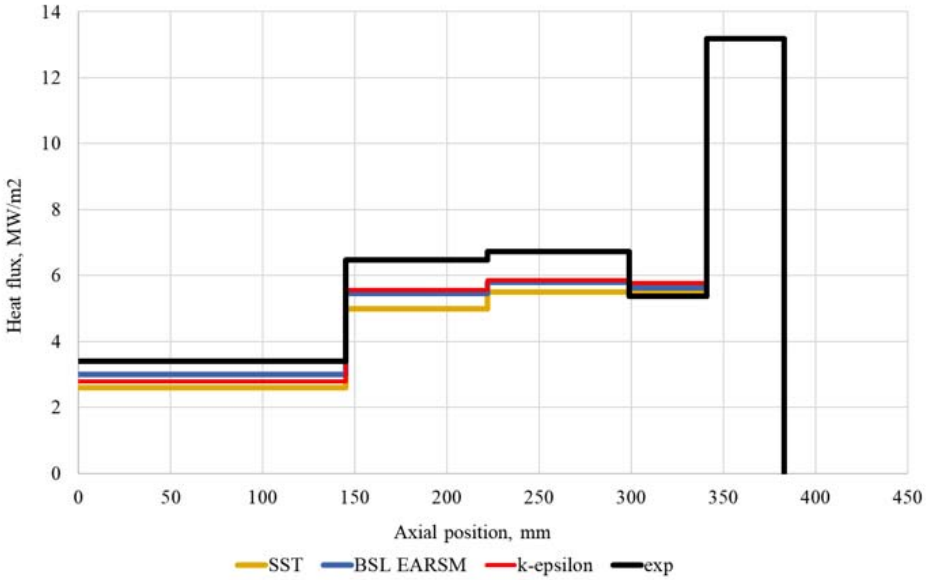

FIGURE 15. Segment average heat flux distribution.

proaches give very similar profiles of segment heat flux, and, consequently, the integral is also almost equal. It is likely that the lack of heat flux is due to unconsidered radiative heat transfer, which was shown in section 4.3 before.

4.6. *General considerations*

As was already mentioned, the Gray spectral model overestimates the wall radiative heat flux giving 30 – 33 % of radiative/total heat flux. It is interesting to notice that this ratio keeps for all cases studied, as well as the WSGG ratio, which varies in the vicinity of 19 – 20 %. This value also corresponds to the amount of RHF which the authors [29] used in their verification study. Despite they used methane/air mixture at 1 bar, the present research shows it can be applied in rocket propulsion simulations.

Apart from that, the BSL EARSM model is accepted as best among turbulence models observed to reproduce the heat flux and pressure. The Flamelet-2 model provided the

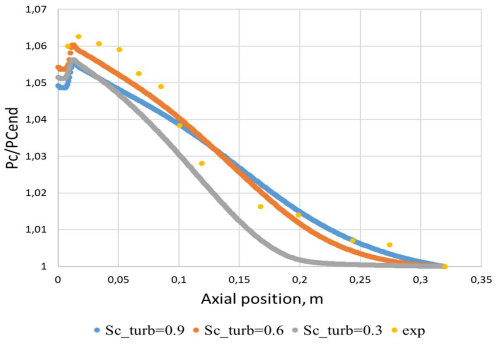

FIGURE 16. Normalized axial pressure distribution.

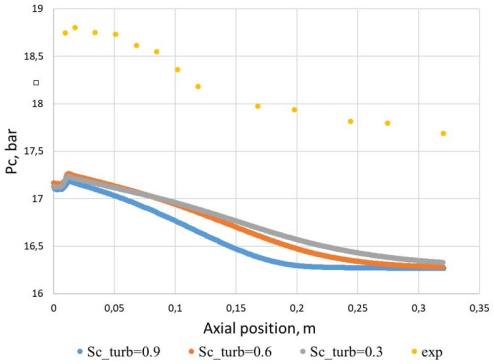

FIGURE 17. Absolute pressure axial distribution.

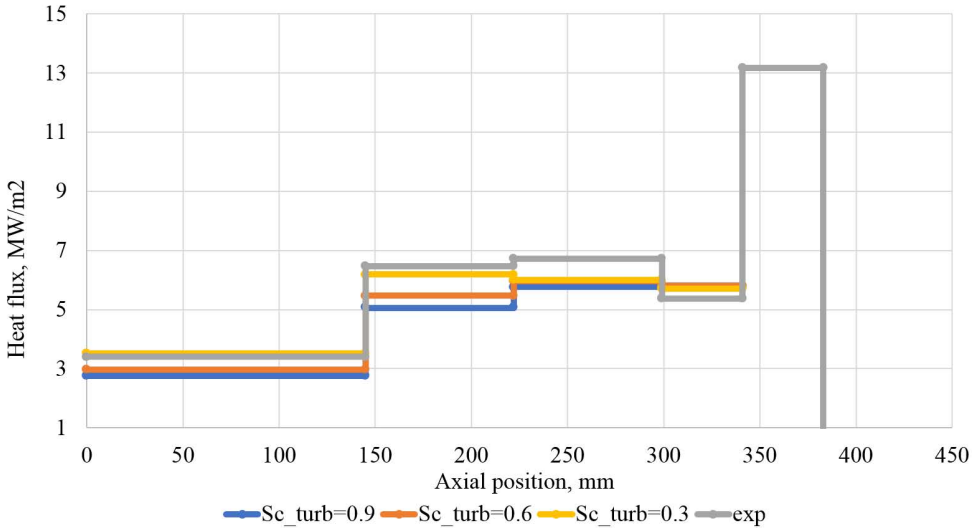

FIGURE 18. Segment average heat flux distribution.

	WSGG	No radiation	exp
Integral, MW	0.177	0.144	0.16
Radiative/Total	0.183		—

TABLE 3. Radiating and non-radiating cases

best fit with experimental pressure and therefore also should be chosen among others. As each studied effect showed some discrepancies and can be unobviously interpreted, a final simulation was proposed to use the chosen models and observe the comparison with the test. Therefore, a calculation with BSL EARSM model for turbulence, Flamelet-2 for combustion and P1 with WSGG for radiation was produced. The default turbulent Prandtl number was applied during the studies. The results of the radiating and non-radiating cases are presented below (Fig. 22- 24).

It is seen that, again, radiation introduces no changes to the normalized pressures.

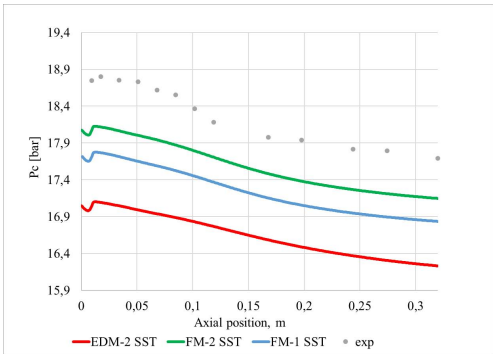

FIGURE 19. Absolute pressure axial distribution.

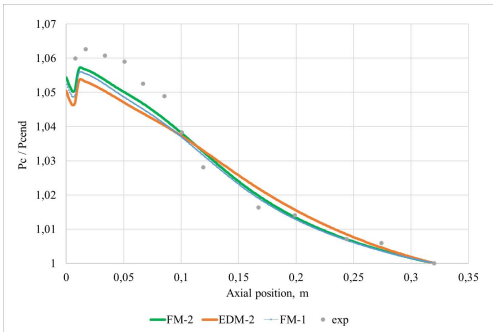

FIGURE 20. Normalized axial pressure distribution.

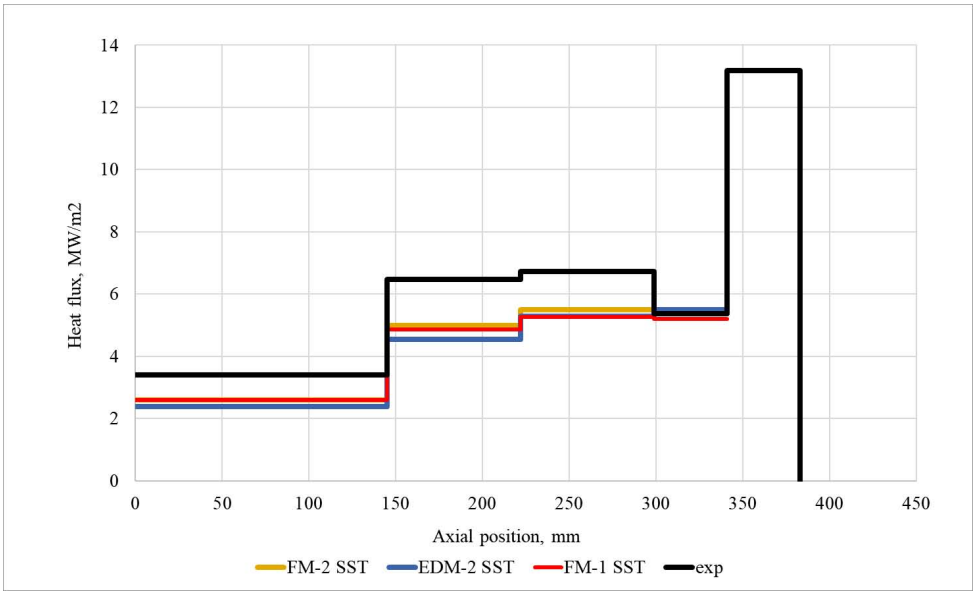

FIGURE 21. Segment average heat flux distribution.

However, the RHF inclusion lowers absolute pressures by around 0.3 bar, which also results in higher average and integral heat flux comparing to the convective case. The radiating case overestimates heat fluxes in the 3 and 4 segment. Perakis et al. [5] showed that for the 4th and the nozzle segment the experimental heat flux estimation had discrepancies between the coupled heat transfer calculations and the calorimetric method. This was addressed to a small deficiency of the experimental estimation. The overestimated heat flux values in the 3rd segment, however, are due to numerical errors in the present study. Overall, inclusion of the WSGG model, application of the 20 bar Flamelet libraries and BSL EARSM turbulence model are considered to give the best fit among the simulations discussed.

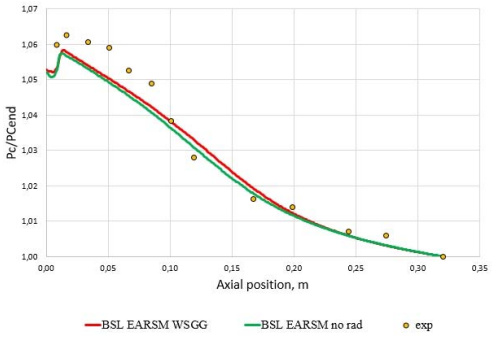

FIGURE 22. Normalized axial pressure distribution.

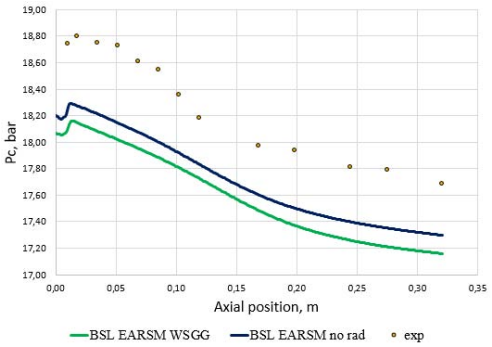

FIGURE 23. Absolute pressure axial distribution.

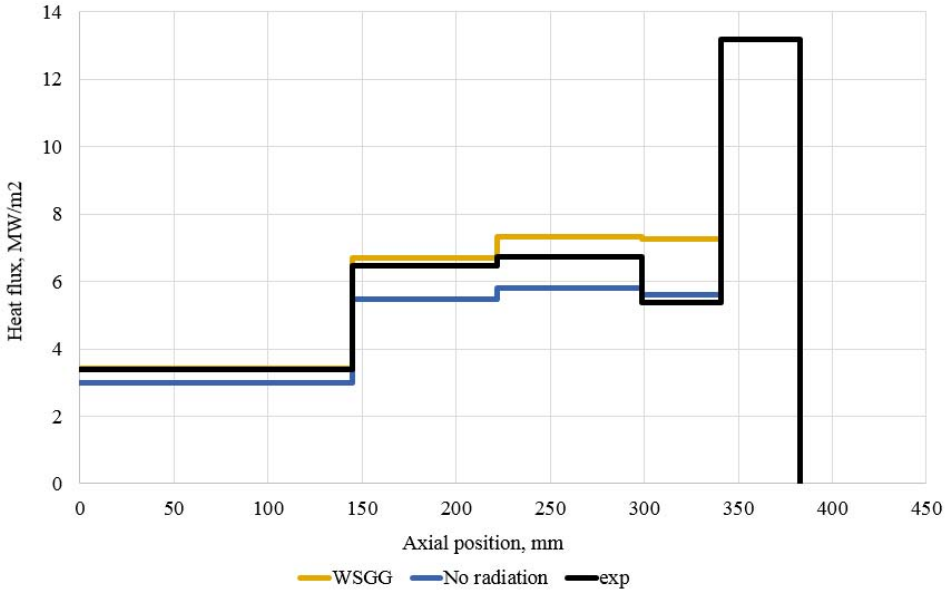

FIGURE 24. Segment average heat flux distribution.

5. Conclusions

Within the SFB-TRR 40 Summer Program 2019 framework several 3D RANS simulations of a seven-element rocket thrust chamber operated at the TUM were produced. For the simulation, different models of physical processes were included and their influence studied. An adiabatic Flamelet with the C1 mechanism and an enhanced EDM approaches were considered for combustion; BSL EARSM, SST and high-Re k-epsilon models were used to model turbulence; variations of the turbulent diffusion closure "sigma" coefficients was applied; several constant turbulent Schmidt and Prandtl numbers were varied and two algebraic variable turbulent Prandtl models were applied to compare; finally, the P1 model with Gray and WSGG approaches was applied to simulate the radiative heat transfer.

It was found that the variable turbulent Prandtl models show similar average values – for the Kays and Crawford the turbulent Prandtl varied in the vicinity of 0.84 . . . 0.89

whereas for the Wassel and Catton it was beetwen 0.87 . . . 0.93. These values and the behavior of the results given are also close to those derived using the constant Pr_t 0.9. This corresponds to the approximations of other researchers and was considered to give a good fit with experimental data. The variable turbulent Prandtl approaches also did not result in any convergence difficulties or high resource requirements and are thus recommended for future application in rocket propulsion simulations as they are suitable for any injection and mixing types. The variable turbulent Schmidt model, which has been implemented, but not used during the project, needs to be studied in future regarding this case.

The BSL EARSM model showed best agreement with the test data both for the pressures and the heat flux among the turbulence approaches employed. This is addressed to the nonlinear term present in the definition of the turbulent stresses and therefore the representation of anisotropy in the near wall areas. This is a question for further research and comparison with some other RSM models in future.

The comparison of the combustion simulation approaches showed that the Flamelet library generated for the initial pressure of 20 bar is most relevant for the present case. It was both good at representation of the pressure fields and the heat fluxes and gave robust and fast performance. The enhanced global reaction eddy-dissipation model gave an error of 8% in pressures, which is acceptable for first engineering estimations, but is still too coarse for further detailed design. The distinction between the two flamelet libraries generated for the 1 and 20 bar reached 0.3 bar which is less than 2% of the experimental pressure. This is interesting from an engineer's point of view as it shows a small effect of the initial pressures for the calculation of integral parameters such as pressure and heat fluxes. This outline should be checked on other geometries, propellants and injection conditions.

Finally, the results showed an overestimation of heat flux with the P1 Gray spectral approximation. This can be improved by the application of WSGG models, as the one used in this study. The implementation of the four-gases WSGG approach gave a radiative/total heat flux ratio of 20% which is more reasonable than 30% provided by the Gray approach. Although the used WSGG needs more verification studies and maybe inclusion of more gray gases to reproduce thin effects, it can be recommended for rocket propulsion. Another important outcome is the need to include the radiative heat flux in the simulations as the resulting wall heat flux field might be underestimated.

The best fit with the test data, both for the normalized/absolute pressures and wall heat fluxes is given by the combination of 20 bar Flamelets, BSL EARSM turbulence model, the Pr_t 0.9, which is nearly equal to the KC or WC variable turbulent Prandtl approaches here, and the P1 WSGG model for radiative heat transfer. The resulting error in absolute pressures is around 2.9%, and the results of the wall heat flux are also sufficiently similar to the experimental ones, taking into account the discrepancies in the 4th segment.

Another important outcome of this research is the possibility to use relatively coarse grids having y^+ corresponding to the logarithmic region, at least for engineering optimization simulations which would result in reasonable results for the pressures and heat flux parameters.

References

[1] SILVESTRI, S., CELANO, M., SCHLIEBEN, G. AND HAIDN, O. (2016). Characterization of a multi-injector GOX-GCH4 combustion chamber. In: *Joint Propulsion Conference. JPC2016*.

[2] SILVESTRI, S., KIRCHBERGER, C., SCHLIEBEN, G., CELANO, M. AND HAIDN, O. (2017). Experimental and numerical investigation of a multi-injector GOX-GCH4 combustion chamber. In: *31st International Symposium on Space Technology and Science (ISTS)*. Japan.

[3] CHUDINA, Y., BOROVIK, I. AND KOZLOV, A. (2017). Design and fire-tests of an oxygen-methane engine with a thrust of 200 N. *PNRPU Aerospace Engineering Bulletin*, **51**.

[4] ANSYS Inc. (2019). *Ansys CFX theory guide*. V. 2019 R2.

[5] PERAKIS, N., RAHN, D., HAIDN, O. AND EIRINGHAUS, D. (2019). Heat transfer and combustion simulation of seven-element O2/CH4 rocket combustor. *Journal of Propulsion and Power*, pp. 1–18.

[6] PERAKIS, N., STRAUS, J. AND HAIDN, O. (2019). Heat flux evaluation in a multi-element CH4/O2 rocket combustor using an inverse heat transfer method. *International Journal of Heat and Mass Transfer*, **142**, 118425. ISSN 0017-9310. DOI https://doi.org/10.1016/j.ijheatmasstransfer.2019.07.075. URL `http://www.sciencedirect.com/science/article/pii/S0017931018361593`.

[7] PERAKIS, N., RAHN, D., EIRINGHAUS, D., DAIMON, Y., ZHANG, S., KARL, S., HORCHLER, T. AND HAIDN, O. (2018). Qualitative and quantitative comparison of rans simulation results for a 7 element GOX/GCH4 rocket combustor. In: *54th AIAA/SAE/ASEE Joint Propulsion Conference*.

[8] ROTH, C., HAIDN, O., CHEMNITZ, A., SATTELMAYER, T., FRANK, G., MUELLER, H., ZIPS, J., KELLER, R., GERLINGER, P. AND MAESTRO, D. (2016). Numerical investigation of flow and combustion in a single element GCH4/GOX rocket combustor. In: *52nd AIAA/SAE/ASEE Joint Propulsion Conference*. p. 4995.

[9] DAIMON, Y., NEGISHI, H., SILVESTRI, S. AND HAIDN, O. (2018). Conjugated combustion and heat transfer simulation for a 7 element GOX/GCH4 rocket combustor. In: *2018 Joint Propulsion Conference*.

[10] CHEMNITZ, A., SATTELMAYER, T., ROTH, C., HAIDN, O., DAIMON, Y., KELLER, R., GERLINGER, P., ZIPS, J. AND PFITZNER, M. (2018). Numerical investigation of reacting flow in a methane rocket combustor: Turbulence modeling. *Journal of Propulsion and Power*, **34**(4), pp. 864–877.

[11] MUTO, D., DAIMON, Y., SHIMIZU, T. AND NEGISHI, H. (2018). Wall modeling of reacting turbulent flow and heat transfer in liquid rocket engines. In: *Joint Propulsion Conference*.

[12] BALARAS, E., BENOCCI, C. AND PIOMELLI, U. (1996). Two-layer approximate boundary conditions for large-eddy simulations. *AIAA Journal*, **34**(6), pp. 1111–1119.

[13] RANI, S., SMITH, C. AND NIX, A. (2009). Boundary-layer equation-based wall model for large-eddy simulation of turbulent flows with wall heat transfer. *Numerical Heat Transfer. Part B: Fundamentals*, **55**(2), pp. 91–115.

[14] KAWAI, S. AND LARSSON, J. (2012). Wall-modeling in large eddy simulation: Length scales, grid resolution, and accuracy. *Physics of Fluids*, **24**.

[15] PIOMELLI, U. (2008). Wall-layer models for large-eddy simulations. *Progress in Aerospace Sciences*, **44**(6), pp. 437–446.

[16] LARSSON, J., KAWAI, S., BODART, J. AND BERMEJO-MORENO, I. (2016). Large eddy simulation with modeled wall-stress: recent progress and future directions. *Mechanical Engineering Reviews*, **3**(1), pp. 1–23.

[17] MAHEU, N., MOUREAU, V., DOMINGO, P., DUCHAINE, F. AND BALARAC, G. (2012). Large-eddy simulations of flow and heat transfer around a low-mach number turbine blade. In: *Proceedings of the Summer Program*. Center for Turbulence Research.

[18] YODER, D. (2016). Comparison of turbulent thermal diffusivity and scalar variance models. In: *54th AIAA Aerospace Sciences Meeting*.

[19] KAYS, W. AND CRAWFORD, M. (1993). *Convective Heat and Mass Transfer*. 3rd edn. McGraw-Hill. New York.

[20] WASSEL, A. AND CATTON, I. (1973). Calculation of turbulent boundary layers over flat plates with different phenomenological theories of turbulence and variable turbulent prandtl number. *International Journal of Heat and Mass Transfer*, **16**(8), pp. 1547–1563.

[21] LONGO, R., BELLEMANS, A., FERRAROTTI, M., DERUDI, M. AND PARENTE, A. (2018). A new turbulent schmidt number formulation based om the local turbulence level. In: *12th International ERCOFTAC Symposium on Engineering Turbulence Modelling and Measurements*. Montpellier.

[22] EHRHARD, J. AND MOUSSIOPOULOS, N. (2000). On a new nonlinear turbulence model for simulating flows around building shaped structures. *Journal of Wind Engineering and Industrial Aerodynamics*, **88**(1), pp. 91–99.

[23] POSCHNER, M. AND PFITZNER, M. (2008). Real gas CFD simulation of supercritical H2-LOX in the MASCOTTE single injector combustor using a commercial CFD code. In: *46th AIAA Aerospace Sciences Meeting and Exhibit*.

[24] MENTER, F. AND LECHNER, R. (2019). *Best Practice: Generalized $k-\omega$ Two-Equation Turbulence Model in ANSYS CFD (GEKO)*. Tech. rep., ANSYS.

[25] (2019). *Ansys Fluent theory guide*. Tech. rep., ANSYS Inc. V. 2019 R2, USA, 15317.

[26] PETERS, N. (1984). Laminar diffusion flamelet models in non-premixed turbulent combustion. *Progress in energy and combustion science*, **10**(3), pp. 319–339. ISSN 0360-1285. DOI https://doi.org/10.1016/0360-1285(84)90114-X. URL http://www.sciencedirect.com/science/article/pii/036012858490114X.

[27] MAGNUSSEN, B. AND HJERTAGER, B. (1977). On mathematical models of turbulent combustion with special emphasis on soot formation and combustion. In: *Symposium (International) on Combustion*, vol. 16. ISSN 0082-0784, pp. 719–729.

[28] THELLMANN, A. (2010). *Impact of Gas Radiation on Viscous Flows, in particular on Wall Heat Loads, in Hydrogen-Oxygen vs. Methane-Oxygen Systems, based on the SSME Main Combustion Chamber*. Ph.D. thesis, Universitaet der Bundeswehr Muenchen.

[29] CENTENO, F., SILVA, C., BRITTES, R. AND FRANCIS, H. (2015). Numerical simulations of the radiative transfer in a 2d axisymmetric turbulent non-premixed methane-air flame using up-to-date WSGG and gray-gas models. *Journal of the Brazilian Society of Mechanical Sciences and Engineering*, **37**(6), pp. 1839–1850. DOI 10.1007/s40430-015-0425-2.